

# TransBTSV2: Wider Instead of Deeper Transformer for Medical Image Segmentation

Jiangyun Li, Wenxuan Wang, Chen Chen, *Member, IEEE*, Tianxiang Zhang,  
Sen Zha, Hong Yu, Jing Wang

**Abstract**—Transformer, benefiting from global (long-range) information modeling using self-attention mechanism, has been successful in natural language processing and computer vision recently. Convolutional Neural Networks, capable of capturing local features, are unable to model explicit long-distance dependencies from global feature space. However, both local and global features are crucial for dense prediction tasks, especially for 3D medical image segmentation. In this paper, we exploit Transformer in 3D CNN for 3D medical image volumetric segmentation and propose a novel network named TransBTSV2 based on the encoder-decoder structure. Different from our original TransBTS [1], the proposed TransBTSV2 is not limited to brain tumor segmentation (BTS) but focuses on general medical image segmentation, providing a strong and efficient 3D baseline for volumetric segmentation of medical images. As a hybrid CNN-Transformer architecture, TransBTSV2 can achieve accurate segmentation of medical images without any pre-training. With the proposed insight to redesign the internal structure of Transformer and the introduced Deformable Bottleneck Module, a highly efficient architecture is achieved with superior performance. Extensive experimental results on four medical image datasets (BraTS 2019, BraTS 2020, LiTS 2017 and KiTS 2019) demonstrate that TransBTSV2 achieves comparable or better results as compared to the state-of-the-art methods for the segmentation of brain tumor, liver tumor as well as kidney tumor. Code is available at <https://github.com/Wenxuan-1119/TransBTS>.

**Index Terms**—Medical Image Segmentation, Transformer, 3D CNN, Brain Tumor, Liver Tumor, Kidney Tumor

## I. INTRODUCTION

As one of the most common clinical diseases, cancer causes numerous deaths every year. The precise measurements from medical images can assist doctors in making accurate diagnosis and further treatment planning. As illustrated in Fig. 1, medical image segmentation aims to identify tumors and delineate different sub-regions of organs from background, by

J. Li, W. Wang, T. Zhang, S. Zha, H. Yu and J. Wang are with the School of Automation and Electrical Engineering, University of Science and Technology Beijing, Beijing 100083, China. (e-mail: leejy@ustb.edu.cn, s20200579@xs.ustb.edu.cn, txzhang@ustb.edu.cn, g20198675@xs.ustb.edu.cn, g20198754@xs.ustb.edu.cn, m2021207-18@xs.ustb.edu.cn)

C. Chen is with the Center for Research in Computer Vision, University of Central Florida, Orlando, FL 32816 USA. (e-mail: chen.chen@crvc.ucf.edu)

Corresponding author: Jiangyun Li.

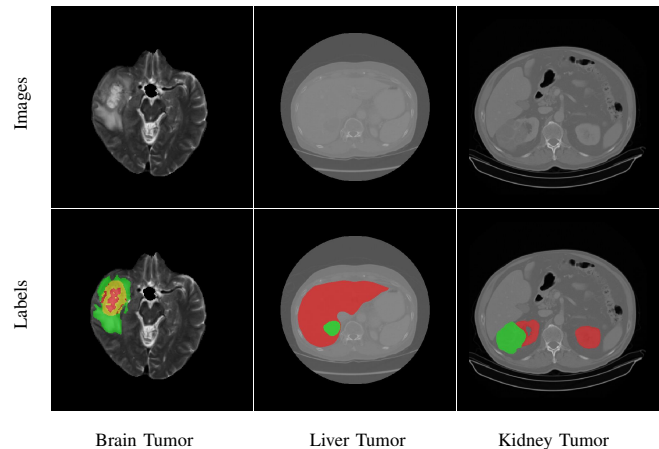


Fig. 1. Examples of medical images with the corresponding semantic segmentation annotations.

assigning a predefined class label to each pixel in medical images, such as Magnetic Resonance Imaging (MRI) [2] and Computerized Tomography (CT) [3]. Traditionally, the lesion regions are mainly delineated by clinicians heavily relying on clinical experiences, which is time-consuming and prone to error. Therefore, for improving the accuracy and efficiency of clinical diagnosis, it is of vital importance to promote the development of automatic medical image segmentation.

Different from natural images, some unique characteristics of medical images make the automatic segmentation task very challenging. First, the shapes and textures of different tumors vary greatly, so it is difficult to find the commonalities between them by direct matching. In addition, some lesions do not have clear boundaries, making it difficult to accurately separate the contours of these tumors. Furthermore, differences of tumor structure in size, extension and location also prevent segmentation algorithms from using strong prior knowledge. Therefore, it is very challenging to automatically and accurately segment medical images.

To tackle the aforementioned problems of medical image segmentation, many approaches have been proposed, including statistical shape models, contour-based approaches and machine learning-based methods [4]–[6]. However, these methods heavily rely on hand-crafted features and have limited feature representation capability. Recently, Convolutional Neural Networks (CNNs) have dominated visual modeling in a

wide range of computer vision tasks. Since local features are essential to clearly segment the boundaries and lesions in medical images, CNNs are quickly adopted for medical image segmentation task. In particular, U-Net [7] adopts a symmetric encoder-decoder structure with skip-connections to refine detail preservation. With the skip-connections and successive upsampling operations in decoder, U-Net can realize the fusion of multi-level features and recover more accurate segmentation edges, becoming the mainstream architecture for medical image segmentation. In the following research, U-Net variants such as U-Net++ [8] and Res-UNet [9] further improve the segmentation performance. However, although CNN-based methods have prominent representation capabilities, it is difficult for CNNs to model explicit **long-distance** dependencies because of limited receptive fields of convolution kernels. This intrinsic limitation of convolution operations prevents CNNs from learning global semantic information, which is critical for dense prediction tasks like segmentation.

Inspired by attention mechanism [10] in natural language processing (NLP), existing research overcome the inherent inability to model long-distance dependencies by fusing the attention mechanism with CNN models. The key idea of the attention mechanism is to model the long-range relationship between feature representations and update feature maps based on the attention weights. Different from convolution, a single attention layer is capable of capturing global semantic information from the whole feature space. For example, non-local neural networks [11] aim to capture the long-distance dependencies in feature maps based on the self-attention mechanism, but suffering from the high memory and computational cost. Since modeling explicit long-range dependencies is crucial for precise segmentation of organs and tumors in medical images, attention mechanism is also widely adopted in medical image segmentation [12], [13], obtaining remarkable results.

Based on self-attention mechanism, Transformer [14], designed to model long-range dependencies in sequence-to-sequence tasks, is able to capture the relations between arbitrary positions in the sequence. Compared to attention mechanism, Transformer is more powerful in modeling global context and possess stronger capability of feature representation attributed to its unique architecture, which is more suitable for overcoming the difficulties of medical image segmentation. Lately, Transformer-based frameworks have reached state-of-the-art performance on various computer vision tasks. For example, Vision Transformer (ViT) architecture [15], [16] has achieved outstanding performance for image classification via pre-training on large-scale datasets. Afterwards, many Transformer-based architectures [17]–[20] have been explored for dense prediction tasks.

Although Transformer-based methods have achieved promising results on various computer vision tasks, training and deploying Transformer is still a great challenge. On the one hand, the original self-attention mechanism in vanilla Transformer leads to  $O(n^2)$  time and space complexity with respect to sequence length. Furthermore, related research usually employ multiple Transformer layers, resulting in unbearable computational cost and memory footprint, especially when the sequence length is extremely long. To

address this issue, many recent research [21]–[24] have focused on reducing the computational complexity of vanilla Transformer. On the other hand, distinct from CNNs, the performance of Transformers heavily depends on the scale of datasets. As Transformers do not possess strong inductive bias as convolution operations, the performance of Transformer is usually inferior to CNNs when the training data is scarce. To alleviate this problem, a number of state-of-the-art methods turn to pre-training on large-scale datasets. However, medical image datasets are generally short of available training samples, making the pre-training of Transformer on medical images impractical.

In this paper, we exploit Transformer in 3D CNN to effectively model local and global features for medical image volumetric segmentation. To fully exploit the merits of both CNN and Transformer, the network encoder first utilizes 3D CNN to extract the volumetric spatial features and downsample the input 3D images at the same time, effectively capturing the local 3D context information and resulting in compact volumetric feature maps. Then each volume is reshaped into a vector (i.e. token) and fed into Transformer for global feature modeling. Finally, the 3D CNN decoder takes the feature embeddings from Transformer as well as the low-level feature representations from skip-connections, and performs progressive upsamplings to predict the full resolution segmentation maps. As a hybrid CNN-Transformer architecture, our TransBTSV2 can perform accurate segmentation of medical images without any pre-training.

Since the conventional design of Transformer-based methods is to repeatedly stack Transformer layers along model depth, the introduction of Transformer brings considerable computational overhead. To address this dilemma, inspired by the inverted design in MobileNetV2 [25], we propose a new insight to pursue wider instead of deeper Transformer architecture (i.e. prefer larger network width over deeper network depth) to improve model efficiency. Following this simple yet effective design scheme, we gradually expand the model width twice in the whole pipeline to achieve an inverted bottleneck alike architecture, which leads to an impressive decrease in model complexity (53.62% reduction in parameters and 27.63% reduction in FLOPs) compared with our original TransBTS [1]. *With only a single Transformer layer*, superior performance is achieved by our highly efficient TransBTSV2.

In addition, the irregular-shape lesions also bring great challenges to medical image segmentation. Due to the fixed geometric structures of CNN basic modules (e.g. convolution and pooling), CNNs are inherently limited to model irregular-shape deformation of lesion regions. In U-Net architecture, feature maps from encoder are more sensitive to the geometry information and essential to the recognition of target areas. To this end, we propose an effective Deformable Bottleneck Module (DBM) at the position of each skip-connection to learn volumetric spatial offsets from the encoder features and adapt to various transformations of segmentation targets. Thus, the feature maps output from DBMs capture more shape-aware local details and the proposed network can generate finer segmentation results of lesions.

Comprehensive experiments are conducted on four bench-

mark datasets for medical volumetric segmentation to shed light on architecture engineering of incorporating Transformer in 3D CNN to unleash the power of both architectures. It is worth noting that TransBTSV2 is a clean and general 3D network (with basic 3D convolutional layers and Transformer blocks) without any complex structures and add-ons. Any effective techniques such as multi-scale feature fusion can be easily plugged into TransBTSV2 to boost the performance.

This work is an extension of our MICCAI version [1]. We make the following important extensions in this paper:

- We propose a new insight to redesign the Transformer block, pursuing a shallower but wider architecture instead of the traditional deeper but narrower architecture. The model complexity is greatly reduced while better performance is also achieved for medical image segmentation.
- We introduce a Deformable Bottleneck Module (DBM) to capture more shape-aware feature representations. With the proposed DBM, our method can generate finer segmentation results of lesion areas.
- Compared with our MICCAI version [1], we present more results on two popular medical image datasets (LiTS 2017 and KiTS 2019) to evaluate the generalization ability of our proposed TransBTSV2. Extensive experimental results on four benchmark datasets for medical volumetric segmentation demonstrate that TransBTSV2 reaches competitive or better performance than previous state-of-the-art methods.

## II. RELATED WORK

We present a brief overview of the related works from two aspects. The first aspect primarily introduces U-Net and its variants on medical image segmentation, while the second aspect reviews the Transformer-based approaches for various vision tasks, especially medical image segmentation.

### A. U-Net and U-Net Variants

Due to the difficulties of medical image segmentation mentioned above, the multi-scale feature fusion and fine-grained local details modeling are both indispensable for an advanced network. To preserve detail information of medical images as much as possible, U-Net [7] adopts a symmetric encoder-decoder architecture with skip connections to gradually restore the downsampled feature maps to original size, thereby achieving pixel-level dense prediction of medical images. In the following research, U-Net based variants attract a lot of attention and are further applied in medical image segmentation. To fully utilize the local information among continuous slices which is also critical for volumetric segmentation, Cicek et al. [26] generalize the U-Net from 2D to 3D by implementing 3D operations, such as 3D convolution and 3D max pooling, for better medical volumetric segmentation. To model long-range distance dependencies, Ozan Oktay [12] proposes a novel attention gate for medical imaging that automatically learns to focus on target structures of varying shapes and sizes. Based on the residual structure of ResNet [27], Residual U-Nets [28]–[30] are also proposed to overcome the difficulty in training deep neural networks. In addition, there are works

[8], [31] aim to enrich the information interaction of feature maps between different levels by improving skip connections.

### B. Transformer-based Approaches

1) *Transformer for Various Vision Tasks*: With the help of pre-training on large-scale datasets, Transformer-based frameworks have reached state-of-the-art performance on various vision tasks recently. Vision Transformer (ViT) [15] splits the image into fixed-size patches and models the correlations between these patches as sequences, achieving satisfactory results. DeiT [16] introduces a knowledge distillation method for training ViT to further improve its performance. DETR [32] treats object detection as a set prediction task using Transformer, which simplifies the object detection process by abandoning the steps of generating anchors and non-maximum suppression. Rethinking semantic segmentation from a sequence-to-sequence perspective, SETR [17] leverages Transformer as the encoder for global feature extraction and achieves superior performance with large-scale pre-training. To construct efficient architecture for segmentation task, SegFormer [33] combines a novel hierarchically structured Transformer encoder with a lightweight multi-layer perceptron (MLP) decoder. Moreover, to further achieve efficient architecture with less redundancy, Swin Transformer [19] gets rid of the global pairwise self-attention mechanism in ViT and proposes a new transformer backbone based on the proposed local-window self-attention mechanism and shifted window scheme, reaching state-of-the-art results on various benchmarks.

2) *Transformer for Medical Image Segmentation*: To explicitly model long-distance dependencies of volumes in medical images, recent research focus on introducing Transformer to medical image segmentation task. TransUNet [34] employs ViT as encoder with large-scale pre-training for medical image segmentation. TransFuse [35] combines Transformer and CNN in parallel to effectively capture global dependencies and spatial details in a much shallower manner. Besides, MedT [36] proposes a Gated Axial-Attention model which applies an additional control mechanism in the self-attention module to extend existing architectures. MISSFormer [37] redesigns the feed-forward network with the Enhanced Transformer Block to enhance long-range dependencies and supplement local context. Meanwhile, the Enhanced Transformer Context Bridge is proposed to model long-range dependencies and local context of the multi-scale features generated by hierarchical transformer encoder. TransAttUnet [38] integrates a new self-awareness attention module with Transformer and proposes Global Spatial Attention module to effectively learn non-local interactions between features of the encoder. Different from these previously proposed 2D methods, we focus on investigating how to effectively and efficiently incorporate Transformer in popular **3D CNNs** to unleash the potential of both networks. Rather than just surpassing the SOTA results with complex designs, our TransBTSV2 is a highly efficient model with superior performance.

## III. METHODOLOGY

In this section, we first briefly introduce the overall architecture of the proposed TransBTSV2 and provide the details of

TransBTSV2 in terms of network encoder and decoder. Then, we present the new insight to redesign the Transformer block to achieve computation efficiency. Finally, we introduce the Deformable Bottleneck Module (DBM) in TransBTSV2 for capturing more shape-aware feature representations.

### A. CNN-Transformer Hybrid Architecture

1) *Overall Architecture of TransBTSV2*: An overview of the proposed TransBTSV2 is presented in Fig. 2. Given an input medical image  $X \in \mathbb{R}^{C \times H \times W \times D}$  with a spatial resolution of  $H \times W$ , depth dimension of  $D$  (# of slices) and  $C$  channels (# of modalities), we first utilize modified 3D CNN to efficiently generate compact feature maps capturing volumetric spatial features, and then leverage the redesigned Transformer encoder to model the long-distance dependencies in a global space. After that, we repeatedly apply the upsampling and convolutional layers to gradually produce a high-resolution segmentation result.

2) *Network Encoder*: Due to the computational complexity of Transformer is quadratic with respect to the number of tokens (i.e. sequence length), directly flattening the input image to sequence as Transformer input is impractical. Therefore, ViT [15] splits an image into fixed-size ( $16 \times 16$ ) patches and then reshapes each patch into a token. Following ViT, the straightforward tokenization is splitting images into 3D patches for volumetric data. However, this simple strategy makes Transformer unable to model the image *local context information across spatial and depth dimensions* for volumetric segmentation. To address this issue, our solution is to employ the  $3 \times 3 \times 3$  convolution blocks with downsampling (strided convolution with stride=2) to gradually encode input images into low-resolution/high-level feature representations  $F \in \mathbb{R}^{K \times \frac{H}{8} \times \frac{W}{8} \times \frac{D}{8}}$  ( $K = 128$ ), which is 1/8 of input dimensions of  $H, W$  and  $D$  (overall stride (OS)=8). In this way, rich local 3D context features are effectively embedded in  $F$ . Then,  $F$  is fed into the Transformer encoder to further learn long-range correlations with global receptive field.

**Feature Embedding of Transformer Encoder.** Given the feature maps  $F$ , a feature expansion module (a  $3 \times 3 \times 3$  convolutional layer) is used to increase the channel dimension from  $K = 128$  to  $d = 512$ , ensuring comprehensive representation of each volume and expanding the internal width of the following Transformer simultaneously. As the Transformer layer expects a sequence as input, we collapse the spatial and depth dimensions into one dimension, resulting in a  $d \times N$  ( $N = \frac{H}{8} \times \frac{W}{8} \times \frac{D}{8}$ ) feature map  $f$  (i.e.  $N$   $d$ -dimensional tokens). To encode the location information that is necessary for segmentation task, we introduce the learnable position encodings and fuse them with the feature map  $f$  by direct addition, creating the feature embeddings as follows:

$$z_0 = f + PE = W \times F + PE \quad (1)$$

where  $W$  is the feature expansion module,  $PE \in \mathbb{R}^{d \times N}$  denotes the position encodings, and  $z_0 \in \mathbb{R}^{d \times N}$  refers to the feature embeddings.

**Transformer Layers.** The Transformer encoder is composed of  $L$  Transformer layers, and each of them has a standard

architecture, consisting of a multi-head self-attention (MHSA) block and a feed-forward Network (FFN). The output of the  $\ell$ -th ( $\ell \in [1, 2, \dots, L]$ ) Transformer layer can be calculated by:

$$z'_{\ell-1} = MHSA(LN(z_{\ell-1})) + z_{\ell-1} \quad (2)$$

$$z_{\ell} = FFN(LN(z'_{\ell-1})) + z'_{\ell-1} \quad (3)$$

where  $LN(*)$  is the layer normalization and  $z_{\ell}$  is the output of  $\ell$ -th Transformer layer.

3) *Network Decoder*: In order to generate full-resolution segmentation results as original 3D image space ( $H \times W \times D$ ), we introduce 3D CNN decoder to perform feature upsamplings and pixel-level segmentation (see the right part of Fig. 2).

**Feature Restoration.** To fit the input dimension of 3D CNN decoder, we design a feature restoration module to project the sequence data back to a standard 4D feature map. Specifically, the output sequence of Transformer  $z_L \in \mathbb{R}^{d \times N}$  is initially reshaped to  $d \times \frac{H}{8} \times \frac{W}{8} \times \frac{D}{8}$ . In order to reduce the computational complexity of decoder, two convolution blocks are employed to reduce the channel dimension from  $d$  to  $K$ . Through these operations, the feature maps  $Z \in \mathbb{R}^{K \times \frac{H}{8} \times \frac{W}{8} \times \frac{D}{8}}$  is obtained, with the same dimension as  $F$  in the feature encoding part.

**Progressive Feature Upsampling.** After the feature mapping, cascaded upsampling operations and convolution blocks are applied to  $Z$  to gradually recover a full resolution segmentation result  $R \in \mathbb{R}^{H \times W \times D}$ . Moreover, skip-connections are employed to fuse the encoder features with the decoder counterparts by concatenation for finer segmentation masks with richer spatial details.

### B. Efficient Transformer: Prefer Wider to Deeper

To cope with the computational overhead brought by Transformer, inspired by inverted bottleneck blocks in MobileNetV2 [25], a new insight of designing Transformer is proposed in this work. In our original TransBTS [1], the number of transformer layers is  $L = 4$  and the Transformer part accounts for 70.81% of model parameters. Thus, shrinking the model size of Transformer is essential for reducing the overall model complexity. Recently, the mainstream design for Transformer-based methods is to pursue a deeper but narrower hierarchical architecture. However, in this paper, we redesign the Transformer architecture to go wider (hidden dimension of feature vectors) instead of deeper (number of transformer layers). First, the number of Transformer layers  $L$  is reduced from 4 to 1 in order to cut down the model size, leading to an impressive decrease in model complexity (54.11% in parameters and 37.54% in FLOPs). However, the remarkable reduction in parameters usually leads to worse feature representations and an inevitable decline in model performance. Therefore, to restore the modeling capability of our model, the internal width of Transformer is gradually expanded twice (as highlighted with red color in Fig. 2). Specifically, we utilize a feature expansion module to enlarge Transformer width at the first time. Then, with an expansion ratio  $E$ , the hidden dimension of  $q$  and  $k$  are expanded to  $d_m$  (i.e.  $d_m = Ed$ ) to further increase the Transformer width.  $v$  remains unchanged (i.e.  $d = 512$ ) to keep the dimensions of input and output consistent.

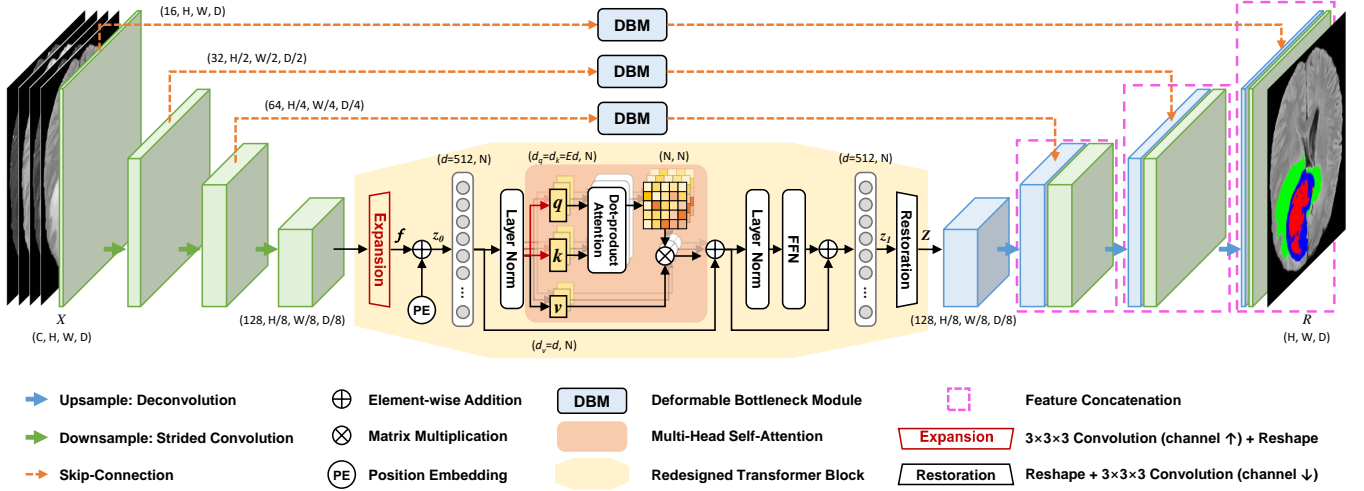


**Fig. 2.** The illustration of the proposed TransBTSV2 for automatic medical image segmentation. We use modified 3D CNN encoder to capture local information and leverage the Transformer encoder to model long-distance dependencies from the global view. Upsampling and convolutional layers are stacked to gradually produce high-resolution segmentation results. We expand the model width twice (as highlighted with red color in the figure) in the whole architecture. With an inverted bottleneck alike Transformer architecture (as highlighted by the yellow shadow in the figure) and the proposed DBM, TransBTSV2 is a highly efficient architecture with superior performance and low model complexity.

As described above, a single scaled dot-product self-attention in Transformer block can be formulated as

$$[q; k; v] = [W_q; W_k; W_v] \times x_i \quad (4)$$

$$W_{atten} = \text{softmax}(q \times k^T / \sqrt{d}) \quad (5)$$

$$x_o = W_{atten} \times v \quad (6)$$

where  $W_q \in \mathbb{R}^{d \times d_m}$ ,  $W_k \in \mathbb{R}^{d \times d_m}$  and  $W_v \in \mathbb{R}^{d \times d}$  are transformation matrices, transferring the input feature embeddings  $x_i \in \mathbb{R}^{N \times d}$  to different dimensional vectors  $q \in \mathbb{R}^{N \times d_m}$ ,  $k \in \mathbb{R}^{N \times d_m}$ , and  $v \in \mathbb{R}^{N \times d}$  respectively. In addition,  $W_{atten} \in \mathbb{R}^{N \times N}$  denotes the attention weights and  $x_o \in \mathbb{R}^{N \times d}$  is the output feature embedding.

In this way, the Transformer block in our model achieves an inverted bottleneck alike architecture (as delineated by the yellow shaded Transformer block in Fig. 2) with greatly reduced model complexity, leading to the proposed highly efficient architecture. Moreover, pursuing the inverted bottleneck alike architecture of Transformer has two advantages. First, the model can learn how to expand the low-dimensional vectors to high dimension space and compress the high-dimensional vectors back to low dimension, making the whole network excellent in scalability and robustness. Second, instead of using low-dimensional vectors to perform matrix operations, computing the self-attention with high-dimensional vectors can improve feature representations of the whole architecture, thus further improving the performance of the model.

### C. Deformable Bottleneck Module

Since the lesion areas in medical images are commonly in irregular shapes with great varieties, it is very challenging to recognize the lesion areas precisely. To achieve better performance in medical image segmentation, it is necessary for the network to capture fine-grained and shape-aware local

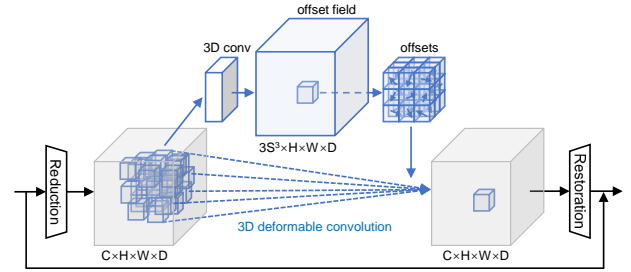


**Fig. 3.** The illustration of the proposed Deformable Bottleneck Module. S refers to the kernel size of the 3D deformable convolution.

details. Due to the fixed geometric structures of CNN basic modules, CNNs are inherently limited to model irregular-shape deformation. To solve this problem, the Deformable Bottleneck Module is designed to further capture shape-aware features from irregular-shape lesion regions. As the feature maps from encoder are more sensitive to geometry information and are essential to the recognition of target areas, the proposed DBMs are plugged right into each skip-connection. Each DBM consists of two  $1 \times 1 \times 1$  convolutions, a  $3 \times 3 \times 3$  deformable convolution and traditional residual connection. In order to minimize the amount of computational overhead brought by the proposed DBM, two  $1 \times 1 \times 1$  convolutions (i.e. Reduction and Restoration layer illustrated in Fig. 3) are deployed to reduce and restore channel dimensions, while the 3D deformable convolution is utilized to capture shape-aware local information. DBMs at each skip-connection can effectively learn volumetric spatial offsets from the encoder features and adapt to various transformations of segmentation targets. Thus, the feature maps output from DBMs provide more shape-aware local details and our proposed TransBTSV2 can generate finer segmentation results of lesion areas. The details of DBM are presented in Fig. 3.

## IV. EXPERIMENTS AND RESULTS

### A. Data and Evaluation Metrics

We evaluate our proposed method on four benchmark datasets for medical volumetric segmentation.

1) *BraTS2019 and BraTS2020*: The first 3D MRI dataset used in the experiments is provided by the Brain Tumor Segmentation (BraTS) 2019 challenge [39]–[41]. It contains 335 cases of patients for training and 125 cases for validation. Each sample is composed of four modalities of brain MRI scans. Each modality has a volume of  $240 \times 240 \times 155$  which has been aligned into the same space. The labels contain 4 classes: background (label 0), necrotic and non-enhancing tumor (label 1), peritumoral edema (label 2) and GD-enhancing tumor (label 4). The performance on the **validation set** assessed by the online evaluation server is used to validate the effectiveness of the proposed method. The segmentation accuracy is measured by the Dice score and the Hausdorff distance (95%) metrics for enhancing tumor region (ET, label 1), regions of the tumor core (TC, labels 1 and 4), and the whole tumor region (WT, labels 1,2 and 4). The second 3D MRI dataset is provided by the Brain Tumor Segmentation (BraTS) 2020 Challenge [39]–[41]. It consists of 369 cases for training, 125 cases for validation and 166 cases for testing. Except for the number of samples in the dataset, the other information regarding these two MRI datasets are the same.

2) *LITS2017*: The third medical image dataset is provided by the Liver Tumor Segmentation (LiTS) 2017 challenge [42]. The LiTS dataset contains 131 and 70 samples of contrast-enhanced 3D abdominal computed tomography scans with annotations of liver and liver tumors for training and testing, respectively. The number of slices ranges from 75 to 987 while the spatial size of each CT image and label is  $512 \times 512$ . The labels contain 3 classes: background (label 0), liver (label 1), liver tumor (label 2). We employ the Dice per case score and Dice global score as evaluation metrics. Dice per case score refers to an average Dice score per volume and Dice global score is the Dice score evaluated by combining the whole datasets into one.

3) *KiTS2019*: The fourth medical image dataset is provided by Kidney Tumor Segmentation (KiTS) 2019 Challenge [43]. KiTS 2019 dataset provides data of multi-phase 3D CTs with high-quality annotated voxel-wise labels for 300 patients. 210 patients were randomly selected for the training set and the remaining 90 patients were the testing set for algorithm evaluation. The ground truth contains 3 classes: background (label 0), kidney (label 1), kidney tumor (label 2). For evaluation of our method, the same three evaluation metrics as KiTS 2019 challenge are used. Kidney dice denotes the segmentation performance when considering both kidneys and tumors as the foreground whereas tumor dice considers everything except the tumors as background. Composite dice is the average of kidney dice and tumor dice.

### B. Implementation Details

The proposed TransBTSV2 is implemented based on Pytorch and trained with NVIDIA Titan RTX GPUs. On the four benchmark datasets, TransBTSV2 is trained from scratch

with a batch size of 16. On **BraTS 2019 and BraTS 2020** datasets, the expansion ratio  $E$  is set to 1.5. The Adam optimizer is adopted to train the model for 6000 epochs. With warm-up strategy for 60 epochs during training, the initial learning rate is set to 0.00008 with a cosine learning rate decay schedule. Random cropping, random mirror flipping and random intensity shift are applied as data augmentation in the training phase. The softmax Dice loss is employed to train the network and  $L2$  Norm is also applied for model regularization with a weight decay rate of  $10^{-5}$ . On **LiTS2017 and KiTS2019** datasets, the expansion ratio  $E$  is set to 2. Adam optimizer is also used to train our method for 6000 epochs and 12000 epochs respectively. With warm-up strategy for 80 epochs and 160 epochs respectively during training, the initial learning rate is set to 0.002 with a cosine learning rate decay schedule. The other aspects of implementation details remain consistent with [44].

### C. Experimental Results

1) *Evaluation on Brain Tumor Segmentation: BraTS 2019*. To fairly evaluate the performance of our proposed TransBTSV2, we first conduct experiments on the BraTS 2019 validation set and compare TransBTSV2 with previous state-of-the-art approaches. The **quantitative results** are presented in Table I. TransBTSV2 achieves the Dice scores of 80.24%, 90.42%, 84.87% and Hausdorff distance of 3.696mm, 5.432mm, 5.473mm on ET, WT, TC respectively, which are comparable or higher results than previous SOTA methods presented in Table I. In terms of Dice scores metric, a considerable improvement has been achieved for segmentation compared with previous SOTA methods. Additionally, it can be seen that TransBTSV2 obtains an absolute dominance over the Hausdorff distance of ET and TC with our redesigned Transformer and DBM. Compared with 3D U-Net [26] that without Transformer as part of encoder, TransBTSV2 shows great superiority in both performance and efficiency with significant improvements. This clearly reveals the benefit of leveraging Transformer for modeling global relationships.

TABLE I

PERFORMANCE COMPARISON ON BRA TS 2019 VALIDATION SET.

Method	Dice Score (%) $\uparrow$			Hausdorff Dist. (mm) $\downarrow$		
	ET	WT	TC	ET	WT	TC
3D U-Net [26]	70.86	87.38	72.48	5.062	9.432	8.719
V-Net [45]	73.89	88.73	76.56	6.131	6.256	8.705
Attention U-Net [12]	75.96	88.81	77.20	5.202	7.756	8.258
Wang et al. [46]	73.70	89.40	80.70	5.994	5.677	7.357
Chen et al. [47]	74.16	90.26	79.25	4.575	4.378	7.954
Li et al. [48]	77.10	88.60	81.30	6.033	6.232	7.409
Frey et al. [49]	78.70	89.60	80.00	6.005	8.171	8.241
Myronenko et al. [50]	80.00	89.40	83.40	3.921	5.89	6.562
Vu et al. [51]	78.42	90.34	81.12	3.700	<b>4.320</b>	6.280
Ahmad et al. [52]	78.56	90.26	83.47	<b>3.591</b>	5.689	7.093
<b>TransBTS [1]</b>	78.93	90.00	81.94	3.736	5.644	6.049
<b>TransBTSV2</b>	<b>80.24</b>	<b>90.42</b>	<b>84.87</b>	3.696	5.432	<b>5.473</b>

For **qualitative analysis**, we show a visual comparison of the brain tumor segmentation results of various methods including 3D U-Net [26], V-Net [45], Attention U-Net [12] and our TransBTSV2 in Fig. 4. Since the ground truth for the validation set is not available, we conduct five-fold cross-validation evaluation on the training set for all methods. It

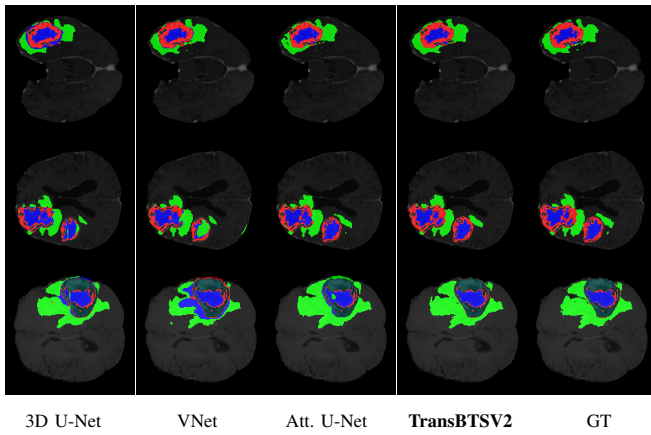


Fig. 4. The visual comparison of MRI brain tumor segmentation results. The blue regions denote the enhancing tumors, the red regions denote the non-enhancing tumors and the green ones denote the peritumoral edema.

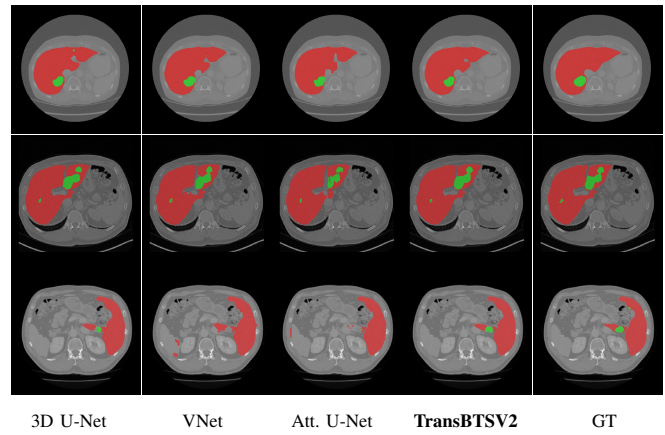


Fig. 5. The visual comparison of CT liver tumor segmentation results. The red regions denote the liver and the green regions denote the tumors.

is apparent from Fig. 4 that TransBTSV2 can segment brain tumors more accurately and generate much better segmentation masks by modeling long-range dependencies between each volume and capturing shape-aware local information.

**BraTS 2020.** We also evaluate TransBTSV2 on BraTS 2020 validation set and the results are reported in Table II. TransBTSV2 achieves Dice scores of 79.63%, 90.56%, 84.50% and Hausdorff distance of 12.522mm, 4.272mm, 5.560mm on ET, WT, TC respectively. Compared with 3D U-Net [26], V-Net [45] and Residual U-Net [9], TransBTSV2 shows great advantages in both metrics with prominent improvements. Moreover, TransBTSV2 reaches competitive or better performance than previous SOTA approaches on BraTS 2020 validation set, demonstrating the potential of our well-designed hybrid architecture. To be mentioned, in comparison with TransBTS [1], great advancements have been made by TransBTSV2 in terms of both metrics on BraTS 2019 and BraTS 2020.

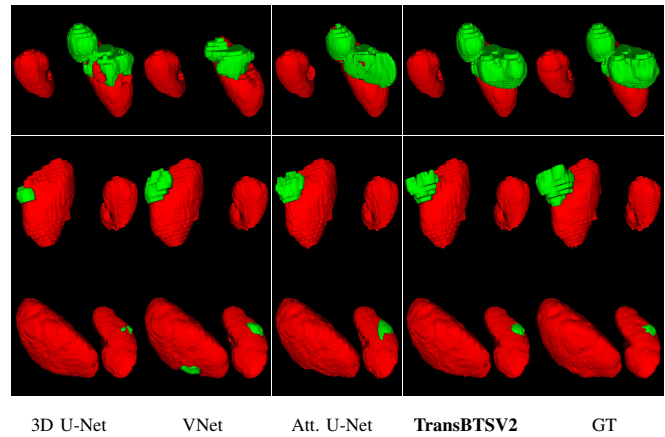


Fig. 6. The visual comparison of CT kidney tumor segmentation results. The red regions denote the kidneys and the green regions denote the tumors.

TABLE II

PERFORMANCE COMPARISON ON BRATS 2020 VALIDATION SET.

Method	Dice Score (%) $\uparrow$			Hausdorff Dist. (mm) $\downarrow$		
	ET	WT	TC	ET	WT	TC
3D U-Net [26]	68.76	84.11	79.06	50.983	13.366	13.607
Basic V-Net [45]	61.79	84.63	75.26	47.702	20.407	12.175
Deeper V-Net [45]	68.97	86.11	77.90	43.518	14.499	16.153
Residual U-Net [9]	71.63	82.46	76.47	37.422	12.337	13.105
Liu et al. [53]	76.37	88.23	80.12	21.390	6.680	6.490
Vu et al. [54]	77.17	90.55	82.67	27.040	4.990	8.630
Fidon et al. [55]	77.60	<b>91.00</b>	84.40	26.800	4.400	5.800
Ghaffari et al. [56]	78.00	90.00	82.00	-	-	-
Nguyen et al. [57]	78.43	89.99	84.22	24.024	5.681	9.566
<b>TransBTS [1]</b>	78.73	90.09	81.73	17.947	4.964	9.769
<b>TransBTSV2</b>	<b>79.63</b>	90.56	<b>84.50</b>	<b>12.522</b>	<b>4.272</b>	<b>5.560</b>

2) *Evaluation on Liver Tumor Segmentation:* To evaluate the performance and generalization ability of TransBTSV2, experiments are also conducted on LiTS 2017 dataset. The performance comparison of evaluation metrics are shown in Table III. It can be found that TransBTSV2 again achieves competitive or better performance across a wide range of metrics compared with SOTA approaches. Especially for the Dice metrics of lesion areas, a considerable improvement is achieved by our TransBTSV2, benefiting from the exploita-

tion of DBM and modified Transformer. For further visual comparison, the segmentation results of different methods are illustrated in Fig. 5. It is evident that the segmentation results of our method are much more close to the ground truth compared with U-Net [26], V-Net [45], and Attention U-Net [12]. With the merits of both Transformers and convolutions, TransBTSV2 can segment liver tumors more precisely and generate finer segmentation results.

TABLE III

PERFORMANCE COMPARISON ON LITS 2017 TESTING SET. (P REFERS TO PRE-TRAINED MODEL)

Method	Lesion (%) $\uparrow$		Liver (%) $\uparrow$	
	Dice per case	Dice global	Dice per case	Dice global
U-Net [58]	65.0	-	-	-
3D DenseUNet w/o P [59]	59.4	78.8	93.6	92.9
2D DenseUNet w/o P [59]	67.7	80.1	94.7	94.7
2D DenseNet w/ P [59]	68.3	81.8	95.3	95.9
2D DenseUNet w/ P [59]	70.2	82.1	95.8	96.3
H-DenseUNet [59]	<b>72.2</b>	82.4	96.1	96.5
I3D [60]	62.4	77.6	95.7	96.0
I3D w/ P [60]	66.6	79.9	95.6	96.2
Han [61]	67.0	-	-	-
Vorontsov et al. [62]	65.0	-	-	-
<b>TransBTSV2</b>	71.2	<b>83.1</b>	<b>96.2</b>	<b>96.6</b>

3) *Evaluation on Kidney Tumor Segmentation*: To further validate the effectiveness and robustness of our method, we conduct experiments on the KiTS 2019 dataset, which provides images and labels of kidneys and lesions with high varieties and complexities. Table IV shows the performance comparison of tumor and kidney segmentation between our method and previous SOTA methods. Compared with Triple-stage 3D U-Net [63], a three-stage architecture with much more model complexity than our TransBTSV2, it can be seen that a remarkable improvement (0.43%) is achieved in terms of the composite dice metric. According to Table IV, TransBTSV2 further enhances the segmentation accuracy for both kidneys and tumors, demonstrating the effectiveness of the well-designed hybrid architecture. To analyze the quality of segmentation results, the 3D displays of kidneys and tumors are shown in Fig. 6. It is clear that with the advantages of exploiting Transformer and the proposed DBM to model long-range dependencies and deformation of irregular shapes, small-scale tumors and relatively large-scale kidneys can be well segmented by our method.

TABLE IV  
PERFORMANCE COMPARISON ON KITS 2019 TESTING SET.

Method	Kidney Dice (%) ↑	Tumor Dice (%) ↑	Composite Dice (%) ↑
U-Net [7]	95.15	82.45	88.80
V-Net [45]	93.70	80.72	87.21
Seg-Net [64]	95.30	82.35	88.83
BiSC U-Net [65]	95.40	74.10	84.75
SE-ResNeXt U-Net [66]	96.80	74.30	85.55
Triple-stage U-Net [63]	96.40	<b>83.80</b>	90.10
Ma [67]	97.34	82.54	89.94
Li [68]	97.17	81.61	89.39
Chen [69]	97.01	81.40	89.20
Mu et al. [70]	97.29	83.21	90.25
<b>TransBTSV2</b>	<b>97.37</b>	83.69	<b>90.53</b>

#### D. Model Complexity

In the MICCAI version [1], our TransBTS is a moderate-size model with 32.99M parameters and 333G FLOPs. With the improved architecture design proposed in this paper, TransBTSV2 only has 15.30M parameters and 241G FLOPs while achieving Dice scores of 80.24%, 90.42%, 84.87% and Hausdorff distance of 3.696mm, 5.432mm, 5.473mm on ET, WT, TC on BraTS2019 validation set. It is worth noting that compared with our original TransBTS [1], pursuing wider instead of deeper Transformer leads to greatly reduced complexity (53.62% reduction in parameters and 27.63% reduction in FLOPs) but significantly improves model performance in the meantime. Compared with 3D U-Net [26] which has 16.21M parameters and 1670G FLOPs, our TransBTSV2 shows great superiority in terms of computational complexity as well as model performance.

#### E. Ablation Study

**Ablation Study for Each Component of our TransBTSV2.** We conduct extensive ablation experiments to verify the effectiveness of TransBTSV2 and justify the rationality of its design based on evaluations on BraTS 2019 validation set. Since there is no testing set provided by the challenge

TABLE V

ABLATION STUDY RESULTS ON BRATS 2019 VALIDATION SET. (B, TR, FEM, DBM, QK↑ REFERS TO BASELINE, TRANSFORMER, FEATURE EXPANSION MODULE, DEFORMABLE BOTTLENECK MODULE, QK LINEAR PROJECTION FOR EXPANDED DIMENSION RESPECTIVELY)

Method	Dice Score (%) ↑			Params(M)	FLOPs(G)
	ET	WT	TC		
B	77.61	89.70	78.97	4.758	158.0
B + TR	79.79	<b>90.55</b>	83.61	5.481	164.0
B + TR + FEM	80.30	90.30	83.84	14.876	208.0
B + TR + FEM + DBM	<b>80.80</b>	90.34	84.00	15.027	235.0
B + TR + FEM + DBM + QK↑	80.24	90.42	<b>84.87</b>	15.304	241.0

organizers, the ablation experiments are performed on official validation set for fair comparison. As illustrated in Table V, compared with our baseline which is a modified 3D U-Net, the hybrid CNN-Transformer architecture shows great superiority on both metrics of Dice scores and Hausdorff distance. This clearly reveals the benefit of leveraging Transformer to model the global relationships. Moreover, employing the proposed DBM makes our TransBTSV2 more powerful to model irregular-shape deformation of lesion regions.

TABLE VI

ABLATION STUDY ON DIFFERENT DESIGNS FOR SPATIAL-SLICE SELF-ATTENTION ON BRATS 2019 VALIDATION SET.

Method	Dice Score (%) ↑			Hausdorff Dist. (mm) ↓		
	ET	WT	TC	ET	WT	TC
joint	<b>80.30</b>	90.30	<b>83.84</b>	3.968	4.435	5.699
split-cascaded	79.09	<b>90.68</b>	83.27	4.161	<b>4.220</b>	5.329
split-parallel	79.33	90.50	83.16	3.689	4.300	5.363
spatial-only	79.27	89.88	82.97	<b>3.463</b>	4.472	<b>5.291</b>

**Ablation Study for Different Designs of Spatial-Slice Self-Attention in Transformer.** We also make a thorough investigation on different designs for spatial-slice self-attention in Transformer. The joint version collectively computes spatial-slice self-attention at the same time, the split version decouples joint attention into spatial attention and slice attention respectively (i.e. spatial Transformer and slice Transformer), and spatial-only denotes only computing self-attention at spatial dimension. Cascaded and parallel represent the relative positions of the two kinds of decoupled Transformer (i.e. spatial Transformer and slice Transformer) mentioned above. As shown in Table VI, the joint version, computing self-attention at spatial and slice dimension simultaneously, achieves better performance than other designs (split version and spatial-only version). A considerable improvement is achieved by the joint version especially on the Dice scores of ET and TC. Although split version and spatial-only version can reduce much memory cost, due to the limited number of tokens (i.e. sequence length) in a single dimension (i.e. spatial or slice), they cannot effectively model explicit long-range dependencies among volumetric spatial features, leading to a sharp decline in model performance.

**Ablation Study for Different Positions of Deformable Bottleneck Module.** In addition, we further analyze the influence of different positions of the DBMs. The experimental results are reported in Table VII. Compared with the architecture without DBM, employing the proposed module on skip-connections brings significant improvements (0.50%) to the



TABLE VII

ABLATION STUDY ON DIFFERENT POSITIONS OF OUR DBM ON BRATS 2019 VALIDATION SET.

Method	Dice Score (%) $\uparrow$			Hausdorff Dist. (mm) $\downarrow$		
	ET	WT	TC	ET	WT	TC
on skip-connections	<b>80.80</b>	<b>90.34</b>	<b>84.00</b>	<b>3.486</b>	4.586	<b>5.272</b>
parallel with MHSA	79.81	90.26	83.89	3.640	5.339	5.549
replace FFN	79.38	90.14	83.91	3.908	<b>4.361</b>	6.126
w/o DBM	80.30	90.30	83.84	3.968	4.435	5.699

dice score of ET, which validates the effectiveness of DBM to capture more shape-aware local details. Moreover, we also experiment with integrating the DBM with Transformer (i.e. parallel with multi-head self-attention or replace the FFN). As shown in Table VII, the resulting networks can not perform as well as before. We speculate that the local features generated by the inserted DBM inside Transformer may interference with the long-range feature modeling of the original Transformer, leading to worse performance.

## V. CONCLUSION

In this paper, we present a novel segmentation framework incorporating Transformer in 3D CNN for volumetric segmentation of medical images. The resulting architecture, TransBTSV2, not only inherits the advantage of 3D CNN for modeling local context information, but also leverages Transformer on learning global semantic correlations. As a hybrid CNN-Transformer architecture, TransBTSV2 can perform accurate segmentation of medical images without any pre-training, possessing the strong inductive bias as CNNs. Experimental results on four medical image datasets demonstrates that the proposed TransBTSV2 is not only highly efficient but also superior or comparable to the performance of previous state-of-the-art methods.

## ACKNOWLEDGMENT

This work was supported by the Fundamental Research Funds for the China Central Universities of USTB (FRF-DF-19-002), Scientific and Technological Innovation Foundation of Shunde Graduate School, USTB (BK20BE014).

## REFERENCES

- [1] W. Wang, C. Chen, M. Ding, H. Yu, S. Zha, and J. Li, "Transbts: Multimodal brain tumor segmentation using transformer," in *International Conference on Medical Image Computing and Computer-Assisted Intervention*. Springer, 2021, pp. 109–119.
- [2] Y. Huo, J. Liu, Z. Xu, R. L. Harrigan, A. Assad, R. G. Abramson, and B. A. Landman, "Robust multicontrast mri spleen segmentation for splenomegaly using multi-atlas segmentation," *IEEE Transactions on Biomedical Engineering*, vol. 65, no. 2, pp. 336–343, 2017.
- [3] H.-G. Nguyen, C. Fouard, and J. Troccaz, "Segmentation, separation and pose estimation of prostate brachytherapy seeds in ct images," *IEEE Transactions on Biomedical Engineering*, vol. 62, no. 8, pp. 2012–2024, 2015.
- [4] Z. Yu-Qian, G. Wei-Hua, C. Zhen-Cheng, T. Jing-Tian, and L. Ling-Yun, "Medical images edge detection based on mathematical morphology," in *2005 IEEE engineering in medicine and biology 27th annual conference*. IEEE, 2006, pp. 6492–6495.
- [5] A. Tsai, A. Yezzi, W. Wells, C. Tempany, D. Tucker, A. Fan, W. E. Grimson, and A. Willisky, "A shape-based approach to the segmentation of medical imagery using level sets," *IEEE transactions on medical imaging*, vol. 22, no. 2, pp. 137–154, 2003.
- [6] K. Held, E. R. Kops, B. J. Krause, W. M. Wells, R. Kikinis, and H.-W. Muller-Gartner, "Markov random field segmentation of brain mr images," *IEEE transactions on medical imaging*, vol. 16, no. 6, pp. 878–886, 1997.
- [7] O. Ronneberger, P. Fischer, and T. Brox, "U-net: Convolutional networks for biomedical image segmentation," in *International Conference on Medical image computing and computer-assisted intervention*. Springer, 2015, pp. 234–241.
- [8] Z. Zhou, M. M. R. Siddiquee, N. Tajbakhsh, and J. Liang, "Unet++: A nested u-net architecture for medical image segmentation," in *Deep learning in medical image analysis and multimodal learning for clinical decision support*. Springer, 2018, pp. 3–11.
- [9] Z. Zhang, Q. Liu, and Y. Wang, "Road extraction by deep residual u-net," *IEEE Geoscience and Remote Sensing Letters*, vol. 15, no. 5, pp. 749–753, 2018.
- [10] D. Bahdanau, K. Cho, and Y. Bengio, "Neural machine translation by jointly learning to align and translate," *arXiv preprint arXiv:1409.0473*, 2014.
- [11] X. Wang, R. Girshick, A. Gupta, and K. He, "Non-local neural networks," in *Proceedings of the IEEE conference on computer vision and pattern recognition*, 2018, pp. 7794–7803.
- [12] O. Oktay, J. Schlemper, L. L. Folgoc, M. Lee, M. Heinrich, K. Misawa, K. Mori, S. McDonagh, N. Y. Hammerla, B. Kainz *et al.*, "Attention u-net: Learning where to look for the pancreas," *arXiv preprint arXiv:1804.03999*, 2018.
- [13] J. Schlemper, O. Oktay, M. Schaap, M. Heinrich, B. Kainz, B. Glocker, and D. Rueckert, "Attention gated networks: Learning to leverage salient regions in medical images," *Medical image analysis*, vol. 53, pp. 197–207, 2019.
- [14] A. Vaswani, N. Shazeer, N. Parmar, J. Uszkoreit, L. Jones, A. N. Gomez, L. Kaiser, and I. Polosukhin, "Attention is all you need," in *Advances in neural information processing systems*, 2017, pp. 5998–6008.
- [15] A. Dosovitskiy, L. Beyer, A. Kolesnikov, D. Weissenborn, X. Zhai, T. Unterthiner, M. Dehghani, M. Minderer, G. Heigold, S. Gelly *et al.*, "An image is worth 16x16 words: Transformers for image recognition at scale," *arXiv preprint arXiv:2010.11929*, 2020.
- [16] H. Touvron, M. Cord, M. Douze, F. Massa, A. Sablayrolles, and H. Jégou, "Training data-efficient image transformers & distillation through attention," *arXiv preprint arXiv:2012.12877*, 2020.
- [17] S. Zheng, J. Lu, H. Zhao, X. Zhu, Z. Luo, Y. Wang, Y. Fu, J. Feng, T. Xiang, P. H. Torr *et al.*, "Rethinking semantic segmentation from a sequence-to-sequence perspective with transformers," in *Proceedings of the IEEE/CVF Conference on Computer Vision and Pattern Recognition*, 2021, pp. 6881–6890.
- [18] W. Wang, E. Xie, X. Li, D.-P. Fan, K. Song, D. Liang, T. Lu, P. Luo, and L. Shao, "Pyramid vision transformer: A versatile backbone for dense prediction without convolutions," *arXiv preprint arXiv:2102.12122*, 2021.
- [19] Z. Liu, Y. Lin, Y. Cao, H. Hu, Y. Wei, Z. Zhang, S. Lin, and B. Guo, "Swin transformer: Hierarchical vision transformer using shifted windows," *arXiv preprint arXiv:2103.14030*, 2021.
- [20] X. Chu, Z. Tian, Y. Wang, B. Zhang, H. Ren, X. Wei, H. Xia, and C. Shen, "Twins: Revisiting the design of spatial attention in vision transformers," in *Thirty-Fifth Conference on Neural Information Processing Systems*, 2021.
- [21] N. Kitaev, L. Kaiser, and A. Levskaya, "Reformer: The efficient transformer," *arXiv preprint arXiv:2001.04451*, 2020.
- [22] I. Beltagy, M. E. Peters, and A. Cohan, "Longformer: The long-document transformer," *arXiv preprint arXiv:2004.05150*, 2020.
- [23] J. Ainslie, S. Ontanon, C. Alberti, V. Cvicek, Z. Fisher, P. Pham, A. Ravula, S. Sanghai, Q. Wang, and L. Yang, "Etc: Encoding long and structured inputs in transformers," *arXiv preprint arXiv:2004.08483*, 2020.
- [24] M. Zaheer, G. Guruganesh, K. A. Dubey, J. Ainslie, C. Alberti, S. Ontanon, P. Pham, A. Ravula, Q. Wang, L. Yang *et al.*, "Big bird: Transformers for longer sequences," in *NeurIPS*, 2020.
- [25] M. Sandler, A. Howard, M. Zhu, A. Zhmoginov, and L.-C. Chen, "Mobilenetv2: Inverted residuals and linear bottlenecks," in *Proceedings of the IEEE conference on computer vision and pattern recognition*, 2018, pp. 4510–4520.
- [26] Ö. Çiçek, A. Abdulkadir, S. S. Lienkamp, T. Brox, and O. Ronneberger, "3d u-net: learning dense volumetric segmentation from sparse annotation," in *International conference on medical image computing and computer-assisted intervention*. Springer, 2016, pp. 424–432.
- [27] K. He, X. Zhang, S. Ren, and J. Sun, "Deep residual learning for image recognition," in *Proceedings of the IEEE conference on computer vision and pattern recognition*, 2016, pp. 770–778.

- [28] Z. Fang, Y. Chen, D. Nie, W. Lin, and D. Shen, "Rca-u-net: Residual channel attention u-net for fast tissue quantification in magnetic resonance fingerprinting," in *International Conference on Medical Image Computing and Computer-Assisted Intervention*. Springer, 2019, pp. 101–109.
- [29] H. Li, A. Zhygallo, and B. Menze, "Automatic brain structures segmentation using deep residual dilated u-net," in *International MICCAI Brainlesion Workshop*. Springer, 2018, pp. 385–393.
- [30] X. Xiao, S. Lian, Z. Luo, and S. Li, "Weighted res-unet for high-quality retina vessel segmentation," in *2018 9th international conference on information technology in medicine and education (ITME)*. IEEE, 2018, pp. 327–331.
- [31] H. Huang, L. Lin, R. Tong, H. Hu, Q. Zhang, Y. Iwamoto, X. Han, Y.-W. Chen, and J. Wu, "Unet 3+: A full-scale connected unet for medical image segmentation," in *ICASSP 2020-2020 IEEE International Conference on Acoustics, Speech and Signal Processing (ICASSP)*. IEEE, 2020, pp. 1055–1059.
- [32] N. Carion, F. Massa, G. Synnaeve, N. Usunier, A. Kirillov, and S. Zagoruyko, "End-to-end object detection with transformers," in *European Conference on Computer Vision*. Springer, 2020, pp. 213–229.
- [33] E. Xie, W. Wang, Z. Yu, A. Anandkumar, J. M. Alvarez, and P. Luo, "Segformer: Simple and efficient design for semantic segmentation with transformers," *arXiv preprint arXiv:2105.15203*, 2021.
- [34] J. Chen, Y. Lu, Q. Yu, X. Luo, E. Adeli, Y. Wang, L. Lu, A. L. Yuille, and Y. Zhou, "Transunet: Transformers make strong encoders for medical image segmentation," *arXiv preprint arXiv:2102.04306*, 2021.
- [35] Y. Zhang, H. Liu, and Q. Hu, "Transfuse: Fusing transformers and cnns for medical image segmentation," *arXiv preprint arXiv:2102.08005*, 2021.
- [36] J. M. J. Valanarasu, P. Oza, I. Hacihaliloglu, and V. M. Patel, "Medical transformer: Gated axial-attention for medical image segmentation," *arXiv preprint arXiv:2102.10662*, 2021.
- [37] X. Huang, Z. Deng, D. Li, and X. Yuan, "Missformer: An effective medical image segmentation transformer," *arXiv preprint arXiv:2109.07162*, 2021.
- [38] B. Chen, Y. Liu, Z. Zhang, G. Lu, and D. Zhang, "Transattunet: Multi-level attention-guided u-net with transformer for medical image segmentation," *arXiv preprint arXiv:2107.05274*, 2021.
- [39] B. H. Menze, A. Jakab, S. Bauer, J. Kalpathy-Cramer, K. Farahani, J. Kirby, Y. Burren, N. Porz, J. Slotboom, R. Wiest *et al.*, "The multimodal brain tumor image segmentation benchmark (brats)," *IEEE transactions on medical imaging*, vol. 34, no. 10, pp. 1993–2024, 2014.
- [40] S. Bakas, H. Akbari, A. Sotiras, M. Bilello, M. Rozycki, J. S. Kirby, J. B. Freymann, K. Farahani, and C. Davatzikos, "Advancing the cancer genome atlas glioma mri collections with expert segmentation labels and radiomic features," *Scientific data*, vol. 4, p. 170117, 2017.
- [41] S. Bakas, M. Reyes, A. Jakab, S. Bauer, M. Rempfler, A. Crimi, R. T. Shinohara, C. Berger, S. M. Ha, M. Rozycki *et al.*, "Identifying the best machine learning algorithms for brain tumor segmentation, progression assessment, and overall survival prediction in the brats challenge," *arXiv preprint arXiv:1811.02629*, 2018.
- [42] P. Bilic, P. Christ, E. Vorontsov, G. Chlebus, H. Chen, Q. Dou, C. Fu, X. Han, P. Heng, J. Hesser *et al.*, "The liver tumor segmentation benchmark (lits)," *arXiv preprint arXiv:1901.04056*, 2019.
- [43] N. Heller, N. Sathianathan, A. Kalapara, E. Walczak, K. Moore, H. Kaluzniak, J. Rosenberg, P. Blake, Z. Rengel, M. Oestreich *et al.*, "The kits19 challenge data: 300 kidney tumor cases with clinical context, ct semantic segmentations, and surgical outcomes," *arXiv preprint arXiv:1904.00445*, 2019.
- [44] F. Isensee, J. Petersen, A. Klein, D. Zimmerer, P. F. Jaeger, S. Kohl, J. Wasserthal, G. Koehler, T. Norajitra, S. Wirkert *et al.*, "nnu-net: Self-adapting framework for u-net-based medical image segmentation," *arXiv preprint arXiv:1809.10486*, 2018.
- [45] F. Milletari, N. Navab, and S.-A. Ahmadi, "V-net: Fully convolutional neural networks for volumetric medical image segmentation," in *2016 fourth international conference on 3D vision (3DV)*. IEEE, 2016, pp. 565–571.
- [46] F. Wang, R. Jiang, L. Zheng, C. Meng, and B. Biswal, "3d u-net based brain tumor segmentation and survival days prediction," in *International MICCAI Brainlesion Workshop*. Springer, 2019, pp. 131–141.
- [47] M. Chen, Y. Wu, and J. Wu, "Aggregating multi-scale prediction based on 3d u-net in brain tumor segmentation," in *International MICCAI Brainlesion Workshop*. Springer, 2019, pp. 142–152.
- [48] X. Li, G. Luo, and K. Wang, "Multi-step cascaded networks for brain tumor segmentation," in *International MICCAI Brainlesion Workshop*. Springer, 2019, pp. 163–173.
- [49] M. Frey and M. Nau, "Memory efficient brain tumor segmentation using an autoencoder-regularized u-net," in *International MICCAI Brainlesion Workshop*. Springer, 2019, pp. 388–396.
- [50] A. Myronenko and A. Hatamizadeh, "Robust semantic segmentation of brain tumor regions from 3d mris," in *International MICCAI Brainlesion Workshop*. Springer, 2019, pp. 82–89.
- [51] M. H. Vu, T. Nyholm, and T. Löffstedt, "Tunet: End-to-end hierarchical brain tumor segmentation using cascaded networks," in *International MICCAI Brainlesion Workshop*. Springer, 2019, pp. 174–186.
- [52] P. Ahmad, H. Jin, R. Alrobaea, S. Qamar, R. Zheng, F. Alnajjar, and F. Aboudi, "Mh unet: A multi-scale hierarchical based architecture for medical image segmentation," *IEEE Access*, vol. 9, pp. 148 384–148 408, 2021.
- [53] C. Liu, W. Ding, L. Li, Z. Zhang, C. Pei, L. Huang, and X. Zhuang, "Brain tumor segmentation network using attention-based fusion and spatial relationship constraint," *arXiv preprint arXiv:2010.15647*, 2020.
- [54] M. H. Vu, T. Nyholm, and T. Löffstedt, "Multi-decoder networks with multi-denoising inputs for tumor segmentation," *arXiv preprint arXiv:2012.03684*, 2020.
- [55] L. Fidon, S. Ourselin, and T. Vercauteren, "Generalized wasserstein dice score, distributionally robust deep learning, and ranger for brain tumor segmentation: Brats 2020 challenge," *arXiv preprint arXiv:2011.01614*, 2020.
- [56] M. Ghaffari, A. Sowmya, and R. Oliver, "Brain tumour segmentation using cascaded 3d densely-connected u-net," *arXiv preprint arXiv:2009.07563*, 2020.
- [57] H. T. Nguyen, T. T. Le, T. V. Nguyen, and N. T. Nguyen, "Enhancing mri brain tumor segmentation with an additional classification network," *arXiv preprint arXiv:2009.12111*, 2020.
- [58] G. Chlebus, H. Meine, J. H. Moltz, and A. Schenk, "Neural network-based automatic liver tumor segmentation with random forest-based candidate filtering," *arXiv preprint arXiv:1706.00842*, 2017.
- [59] X. Li, H. Chen, X. Qi, Q. Dou, C.-W. Fu, and P.-A. Heng, "H-denseunet: hybrid densely connected unet for liver and tumor segmentation from ct volumes," *IEEE transactions on medical imaging*, vol. 37, no. 12, pp. 2663–2674, 2018.
- [60] J. Carreira and A. Zisserman, "Quo vadis, action recognition? a new model and the kinetics dataset," in *proceedings of the IEEE Conference on Computer Vision and Pattern Recognition*, 2017, pp. 6299–6308.
- [61] X. Han, "Automatic liver lesion segmentation using a deep convolutional neural network method," *arXiv preprint arXiv:1704.07239*, 2017.
- [62] E. Vorontsov, A. Tang, C. Pal, and S. Kadoury, "Liver lesion segmentation informed by joint liver segmentation," in *2018 IEEE 15th International Symposium on Biomedical Imaging (ISBI 2018)*. IEEE, 2018, pp. 1332–1335.
- [63] X. Hou, C. Xie, F. Li, J. Wang, C. Lv, G. Xie, and Y. Nan, "A triple-stage self-guided network for kidney tumor segmentation," in *2020 IEEE 17th International Symposium on Biomedical Imaging (ISBI)*. IEEE, 2020, pp. 341–344.
- [64] A. Myronenko, "3d mri brain tumor segmentation using autoencoder regularization," in *International MICCAI Brainlesion Workshop*. Springer, 2018, pp. 311–320.
- [65] C. Wang, Y. He, X. Qi, Z. Zhao, G. Yang, X. Zhu, S. Zhang, J.-L. Dillenseger, and J.-L. Coatrieux, "Bisc-unet: A fine segmentation framework for kidney and renal tumor," in *2019 Kidney Tumor Segmentation Challenge: KiTS19, Miccai 2019*. University of Minnesota Libraries Publishing, 2019.
- [66] X. Xie, L. Li, S. Lian, S. Chen, and Z. Luo, "Seru: A cascaded seresnext u-net for kidney and tumor segmentation," *Concurrency and Computation: Practice and Experience*, vol. 32, no. 14, p. e5738, 2020.
- [67] J. Ma, "Solution to the kidney tumor segmentation challenge 2019," 2019, Accessed on: Dec. 10, 2021. [Online]. Available: [http://results.kits-challenge.org/miccai2019/manuscripts/junma\\_1.pdf](http://results.kits-challenge.org/miccai2019/manuscripts/junma_1.pdf).
- [68] Y. Li, "Fully automatic segmentation of kidney and tumor based on cascaded u-nets," 2019, Accessed on: Dec. 10, 2021. [Online]. Available: <http://results.kits-challenge.org/miccai2019/manuscripts/YuL1.1e.pdf>.
- [69] B. Chen, "Segmentation of ct kidney and kidney tumor by mdd-net," 2019, Accessed on: Dec. 10, 2021. [Online]. Available: [http://results.kits-challenge.org/miccai2019/manuscripts/rzchen\\_xmu\\_5.pdf](http://results.kits-challenge.org/miccai2019/manuscripts/rzchen_xmu_5.pdf).
- [70] G. Mu, Z. Lin, M. Han, G. Yao, and Y. Gao, "Segmentation of kidney tumor by multi-resolution vb-nets," 2019, Accessed on: Dec. 10, 2021. [Online]. Available: [http://results.kits-challenge.org/miccai2019/manuscripts/gr\\_6e.pdf](http://results.kits-challenge.org/miccai2019/manuscripts/gr_6e.pdf).